Assessing the oceanic control on the amplitude of sea surface cooling induced by tropical cyclones

Emmanuel M. Vincent,[1] Matthieu Lengaigne,[1] Jérôme Vialard,[1] Gurvan Madec,[1,2] Nicolas C. Jourdain,[3] and Sébastien Masson[1]

Received 24 October 2011; revised 28 March 2012; accepted 30 March 2012; published 15 May 2012.

[1] Tropical cyclones (TCs) induce sea surface cooling that feeds back negatively on their intensity. Previous studies indicate that the cooling magnitude depends on oceanic conditions as well as TC characteristics, but this oceanic control has been poorly documented. We investigate the oceanic influence on TC-induced cooling using a global ocean model experiment that realistically samples the ocean response to more than 3,000 TCs over the last 30 years. We derive a physically grounded oceanic parameter, the Cooling Inhibition index (CI), which measures the potential energy input required to cool the ocean surface through vertical mixing, and hence accounts for the pre-storm upper-ocean stratification resistance to TC-induced cooling. The atmospheric control is described using the wind power index (*WPi*), a proxy of the kinetic energy transferred to the ocean by a TC, which accounts for both the effects of maximum winds and translation speed. The cooling amplitude increases almost linearly with *WPi*. For a given *WPi*, the cooling amplitude can however vary by an order of magnitude: a strong wind energy input can either result in a 0.5°C or 5°C cooling, depending on oceanic background state. Using an oceanic parameter such as CI in addition to wind energy input improves statistical hindcasts of the cold wake amplitude by ∼40%. Deriving an oceanic parameter based on the potential energy required to cool the ocean surface through vertical mixing is thus a promising way to better account for ocean characteristics in TCs studies.

Citation: Vincent, E. M., M. Lengaigne, J. Vialard, G. Madec, N. C. Jourdain, and S. Masson (2012), Assessing the oceanic control on the amplitude of sea surface cooling induced by tropical cyclones, *J. Geophys. Res.*, *117*, C05023, doi:10.1029/2011JC007705.

1. Introduction

[2] Tropical cyclones (TCs) are one of the most destructive natural disasters known to man. Accurately forecasting their intensity is a key to mitigating their huge human and financial costs. Most of the kinetic energy lost by TCs is dissipated by friction at the air-sea interface [*Emanuel*, 2003]. This friction is a source of kinetic energy for the ocean and drives strong upper-layer currents. The resulting oceanic vertical shear triggers instabilities that mix warm surface water with colder water below. This is by far the dominant mechanism contributing to the sea surface temperature (SST) cooling observed in the wake of TCs. By contrast, air-sea heat fluxes play a much smaller role [*Price*, 1981; *Jacob et al.*, 2000; *Vincent et al.*, 2012]. TCs primarily draw their energy from evaporation at the surface of the ocean [*Riehl*, 1950]. While higher ambient SSTs provide the potential for stronger tropical cyclones, the SST cooling under the storm eye is the oceanic parameter to which cyclone intensity is most sensitive [*Schade*, 2000]. TC-induced cooling limits evaporation, thereby resulting in a negative air-sea feedback [*Cione and Uhlhorn*, 2003]. For instance, a modest 1°C cooling can lead to a ∼40% decrease in surface enthalpy fluxes [*Cione and Uhlhorn*, 2003], while a 2.5°C decrease seems sufficient to shut down energy production entirely [*Emanuel*, 1999]. *Emanuel et al.* [2004] demonstrated that coupling a single-column ocean model to a simple axisymmetric hurricane model did clearly improve intensity forecasts of a few selected storms, suggesting that further improvement in operational TC intensity forecasts may be achieved by taking the surface cooling feedback into account. Using a coupled hurricane-ocean model, *Schade and Emanuel* [1999] showed that the surface cooling feedback can reduce TC intensity by more than 50%; the intensity of this feedback depending on the storm translation speed and oceanic parameters such as the mixed layer depth and upper ocean stratification.

[3] Past case studies have illustrated the influence of subsurface oceanic background conditions onto the amplitude of the TC-induced cooling and related TCs intensification [e.g., *Cione and Uhlhorn*, 2003; *Jacob and Shay*, 2003; *Shay and Brewster*, 2010; *Lloyd and Vecchi*, 2011]. These studies

[1]LOCEAN, IRD/CNRS/UPMC/MNHN, Paris, France.
[2]NOC, Southampton, UK.
[3]LEGI, CNRS/UJF/INPG, Grenoble, France.

Corresponding author: E. M. Vincent, LOCEAN, IRD/CNRS/UPMC/MNHN, Tour 45-55 4ème 4, Place Jussieu, Paris F-75252 CEDEX 05, France. (emvincent@phare.normalesup.org)

0148-0227/12/2011JC007705

indeed suggest that the TC-induced mixing is particularly efficient in cooling the ocean surface when the mixed layer is shallow and/or the upper temperature profile is strongly stratified. These conditions often results in a small Ocean Heat Content (OHC) [*Leipper and Volgenau*, 1972], a commonly used metric of TC sensitivity to the ocean subsurface calculated as the temperature integral from the surface down to the 26°C isotherm depth. Further support for oceanic control on TC-induced cooling arises from observations of TCs intensification over the passage of a warm loop current or warm core ring allowing an increase of the ocean to atmosphere enthalpy flux [e.g., *Jacob and Shay*, 2003; *Ali et al.*, 2007]. A well-documented example of the oceanic impact onto TC intensity is the Hurricane Opal (1995) that rapidly intensified as it crossed a warm core ring in the Gulf of Mexico, unexpectedly increasing from Category 1 to Category 4 in 14 h [*Shay et al.*, 2000; *Bosart et al.*, 2000; *Hong et al.*, 2000]. *Lloyd and Vecchi* [2011] illustrated this influence of the upper-ocean stratification on the TCs' intensity evolution on a global basis. *Lloyd et al.* [2011] further showed that the performance of an operational hurricane forecasting system can be improved by a better representation of the horizontal structure of upper-ocean stratification. These findings are also confirmed by the improvements in statistical intensity forecasting resulting from the simple inclusion of OHC as a supplementary predictor [*DeMaria et al.*, 2005; *Mainelli et al.*, 2008]. However, these improvements are still modest, reducing the intensity forecast errors by ∼5%, on average. In a recent review, *Goni et al.* [2009] underlined the need to adequately investigate and quantify the role of the upper ocean in TC intensification and to improve oceanic metrics of cyclone air-sea interactions. *Cione and Uhlhorn* [2003] underlined that under most TCs conditions, the upper-ocean heat content is at least an order of magnitude greater than the energy actually extracted by the storm, suggesting that OHC may not be the most appropriate parameter to account for the upper-ocean effect on TC intensity. *Price* [2009] also suggested that a metric based on a vertical average of temperature would be more relevant for cyclone-ocean interaction studies than a metric based on vertically integrated temperature (such as OHC) as it better reflects the way TCs interact with the ocean.

[4] The ocean influences TCs through changes in SST. *Schade* [2000] argued that the SST effect can be split into two distinct contributions: the ambient SSTs ahead of the storm and the SST cooling induced by the storm under the eyewall. Satellite observations accurately capture the ambient SST ahead of the storm but do not provide reliable estimates of inner-core SST due to intense rainfall [*Wentz et al.*, 2000]. The usefulness of a metric of the oceanic influence on the TC should therefore be measured through its ability to quantify the amplitude of the storm-induced cooling. While idealized studies (such as *Schade and Emanuel*, 1999) already demonstrated that oceanic conditions can modulate the amplitude of the negative air-sea feedback on TCs, they did not propose an integrated oceanic parameter that accounts for this control. Our goal in this paper is hence to derive a simple, physically based measure of the control of oceanic vertical stratification on the surface cooling under TCs conditions and to assess by how much the oceanic vertical stratification modulates the CW magnitude.

[5] The limited number of sub-surface observations under TCs (especially in the inner core region) prevents a direct and precise quantification of the influence of the upper ocean structure on the TC-induced cooling at a global scale from observations alone. While dedicated field campaigns [*Chen et al.*, 2007] and autonomous profilers [*Roemmich et al.*, 2009] now provide access to ocean sub-surface data in the cyclone's vicinity, they do not sample the widely varied oceanic conditions over which TCs transit. As suggested by *Goni et al.* [2009], numerical modeling can provide a useful indirect methodology to investigate the oceanic control of the amplitude of the TC-induced cooling. In this paper, we use an Ocean General Circulation Model (OGCM) driven by TC wind-forcing from an historical TC database, that samples the ocean response to more than 3000 TCs over the last 30 years. The realism of the simulated TC-induced cooling in this data set has been extensively validated in a companion paper [*Vincent et al.*, 2012]. This simulation hence provides a comprehensive data set, allowing in-depth analysis of the influence of a wide spectrum of realistic oceanic stratifications on TC-induced cooling.

[6] The paper is organized as follow. Section 2 presents our strategy to include TC wind-forcing in our OGCM. In section 3, we lay out the physical concept and idealized analytical approach that justify two simple (one oceanic and one atmospheric) parameters that account for the amplitude of the TC-induced cooling. Based on the use of these indices, section 4 quantifies the role of the ocean stratification in modulating the cooling amplitude. This section further describes the improvement brought by accounting for the CI index in predicting the cooling and compares this index to other recently suggested alternatives to the OHC [*Price*, 2009; *Buarque et al.*, 2009; *Lloyd and Vecchi*, 2011]. Section 5 provides a summary of our results as well as a discussion of their implications.

2. Methods

2.1. Data

[7] Observed TCs positions and intensities are derived from the International Best Track Archive for Climate Stewardship (IBTrACS) [*Knapp et al.*, 2010]. The observed SST response to tropical cyclones (TCs) is characterized using the optimally interpolated blend of Tropical Rainfall Measuring Mission (TRMM) Microwave Imager (TMI) and Advanced Microwave Scanning Radiometer AMSR-E SST daily data set over 1998–2007. Despite its inability to provide SST data under heavy precipitation, TMI and AMSR-E provide observations of SST beneath clouds a few days before and after a TC's passage.

2.2. Experimental Design and Model Validation

[8] The model configuration, strategy to include the TC wind-forcing and the experiments analyzed in the present paper have been extensively described and validated in *Vincent et al.* [2012]. The following section provides a short summary of this modeling framework and of the validation of TC-induced cooling.

[9] We use an OGCM configuration built from the NEMO framework [*Madec*, 2008], with 1/2° horizontal resolution and 46 levels (10 m resolution in the upper 100 m). The mixed layer dynamics are represented by an improved Turbulent Kinetic Energy (TKE) closure scheme [*Madec*, 2008]. This configuration successfully reproduces tropical

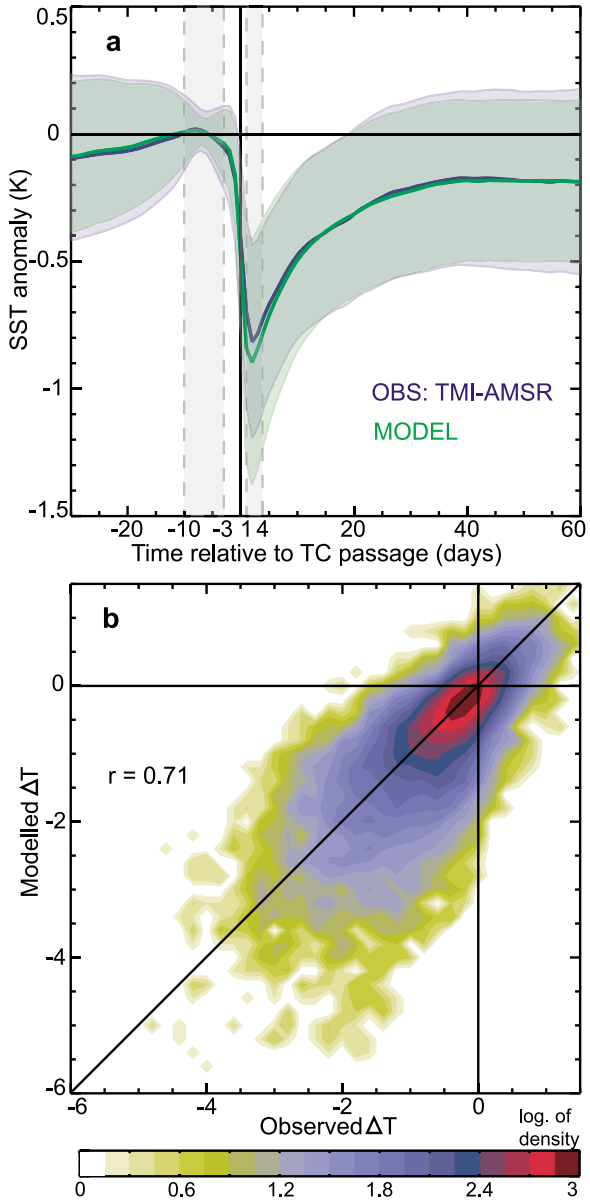

Figure 1. (a) Composite SST evolution averaged under all TCs in observations (blue) and in the model (green). Anomalies are calculated with respect to average pre-storm SST time (days −10 to −3) over a 200 km radius from the TC's position. Day 0 refers to the time when the TC reaches the track position. Color shading shows the ±1/2 standard deviation around the mean composite value. (b) Probability density function of modeled versus observed ΔT due to the passage of the TC: SST averaged over day +1 to day +4 less the SST averaged over day −10 to day −3. The validation samples 1100 storms over the 1998–2007 period (both figures are from *Vincent et al.* [2012]).

ocean variability at intraseasonal to interannual time scales [*Penduff et al.*, 2010; *Lengaigne et al.*, 2012], and is able to simulate TC-induced cooling reasonably well [*Vincent et al.*, 2012]. *Vincent et al.* [2012] show in particular that the 1/2° resolution is a good compromise between accuracy and numerical cost for a realistic global simulation of the ocean response to TCs, thanks to the high temporal resolution of the wind-forcing that allows each grid point to properly sample the wind sequence during TC passage.

[10] The model starts from an ocean at rest, initialized with temperature and salinity fields from the World Ocean Atlas 2005 [*Locarnini et al.*, 2006]. It is then spun up for a 30-year period using the CORE-II bulk formulae and interannual forcing data set (1948–1977) [*Large and Yeager*, 2009; *Griffies et al.*, 2009]. The final state is then used to start the simulations described below, which are run over 1978–2007.

[11] The CORE-II forcing data set does not resolve intense winds associated with tropical cyclones, but contains weaker than observed TC wind signatures. The cyclone free simulation (FILT) is forced by the original interannual CORE forcing from which TC-like vortices are filtered out by applying an 11-day running mean to the wind within 600 km of each cyclone track position (a smooth transition zone, between 600 km and 1,200 km, is also prescribed). The cyclone simulation (CYCL) is forced by realistic TC-wind signatures superimposed to FILT forcing. The 6-hourly cyclone position and strength of the 3,000 named TC between 1978 and 2007 from IBTrACS database [*Knapp et al.*, 2010] are interpolated to the model time step (i.e., every 36 min). This information is used to reconstruct the 10-m wind vector from an idealized TC wind vortex fitted to observations [*Willoughby et al.*, 2006]. A more detailed description of this forcing strategy can be found in *Vincent et al.* [2012].

[12] Our model reproduces the average observed cooling within 200 km of TC tracks quite realistically (Figure 1a). The average maximum cooling for all observed cyclones between 1998 and 2007 is about 1°C in both model and observations. SST starts cooling 3 days prior to the TC passage, and the maximum cooling occurs in its wake of the TC after the passage of the eye. Hereafter, we define the cold wake amplitude ΔT_{CW} as the difference between the wake (days 1 to 3) and the pre-storm (days −10 to −3) SST average values (Figure 1a). We also define the cooling under the eye ΔT_{eye}, as the difference between the eye (12 h before to 12 h after the cyclone passage) and the pre-storm SST (days −10 to −3) average values.

[13] There is a 0.71 correlation between modeled and observed ΔT_{CW} at individual locations (Figure 1b), indicating that our simulation realistically samples the ocean response to the wide spectrum of TC characteristics. The model also successfully reproduces the observed spatial distribution of the cold wake amplitude (see *Vincent et al.* [2012] for more details about the model validation).

3. Introducing a Metric of Oceanic Control of TC-Induced Cooling

[14] In this section, we introduce the basic physical concepts behind our approach. We derive two indices, using analytical calculations from a highly idealized case, to describe the expected dependence of the cooling amplitude to the TC and ocean characteristics.

3.1. Physical Basis

[15] Cooling under TCs largely results from mixing, i.e., from the conversion of kinetic energy to potential energy [*Price*, 1981]. The kinetic energy transferred to the ocean results from the work of surface wind stress on ocean

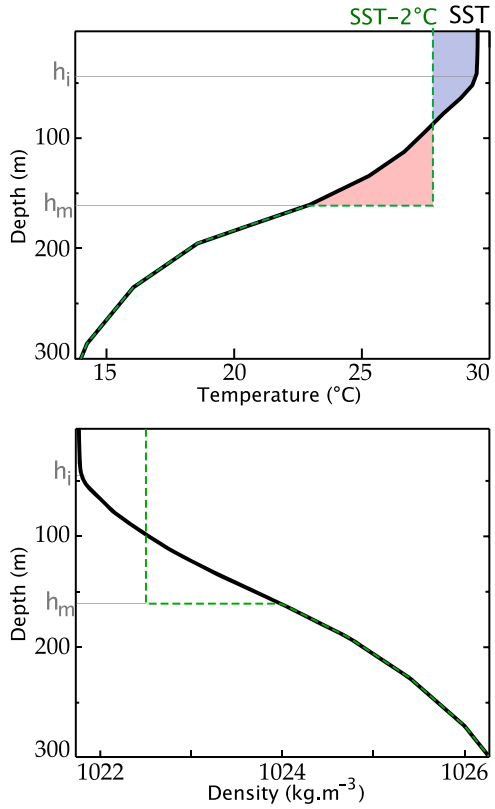

Figure 2. Typical tropical temperature and density profiles before the storm passage (black) and after an idealized heat and mass conserving mixing (dashed green line) used for calculation of the Cooling Inhibition.

currents. The strong resulting currents are driving mixing through strong vertical shear that promotes instabilities. Most of the energy transferred to the ocean radiates away in the surface waves field but a fraction of the kinetic energy is converted into potential energy [*Liu et al.*, 2008]. Warm, light particles are indeed displaced downward while cold, denser particles are displaced upward leading to an increase of the water column potential energy. Based on these simple considerations, a simple relation between the cooling and change in potential energy is derived as follows.

[16] Let us consider an ocean with a linear equation of state depending on temperature only: $\rho(z) = \rho_0(1 - \alpha\, T(z))$. We present here a very simple case with constant stratification N^2, all the way up to the surface. The temperature profile is $T(z) = T_i + \frac{N^2}{\alpha g} z$. Let us now assume that the surface layer has been homogeneously mixed down to the depth h_m, at the temperature T_f.

[17] Conservation of heat yields an equation linking h_m with the surface cooling ΔT

$$h_m + 2\,\frac{\alpha g}{N^2}\Delta T = 0. \tag{1}$$

The potential energy difference between the initial and final profile (ΔE_p) provides an equation linking h_m, ΔT and ΔE_p

$$h_m^3 + \frac{3}{2}\,\frac{\alpha g}{N^2}\Delta T\, h_m^2 = 3\,\frac{\Delta E_p}{\rho_0 N^2}. \tag{2}$$

By combining equations (1) and (2), we obtain an equation linking the cooling and the increase of potential energy of the water column

$$\Delta T = -\frac{1}{\alpha g}\left(\frac{3\,N^4}{2\,\rho_0}\Delta E_p\right)^{1/3}. \tag{3}$$

[18] In the idealized framework above, the surface cooling ΔT is associated to an increase of the water column potential energy ΔE_p and ΔT scales as the cube root of this potential energy increase. Calculations using a more realistic temperature profile that includes a mixed layer are provided in section A1. These calculations show that the relationship found in the simple case above (where the initial mixed layer depth vanishes) remains valid when the initial mixed layer is shallower than a characteristic mixing length. For deeper initial mixed layer, ΔT scales linearly with the potential energy increase ΔE_p. In our simulation, we found that the mixed layer before the cyclone passage is shallower than the characteristic mixing length in ~80% of the cases (Figure A2). This motivates the definition of an oceanic metric based on the cube root of a potential energy change in the next paragraph.

3.2. A Metric of Oceanic Control of TC-Induced Cooling

[19] Given a pre-storm upper-ocean density profile, one can calculate the potential energy increase $\Delta E_p(\Delta T)$ necessary to produce a given ΔT cooling assuming heat conservation and a perfectly homogeneous mixed layer after the mixing (as we did in the idealized case of section 3.1, but this time with the actual profile before the storm). The larger this ΔE_p, the more energy has to be injected into the ocean to produce this cooling. The idea is thus to characterize the propensity of the pre-storm ocean state to yield a weak or strong surface cooling in response to a surface kinetic energy input.

[20] The mixing depth h_m that is necessary to produce a cooling ΔT is first computed from the equation of conservation of heat (see the example with a model profile, for a ΔT of −2°C, on Figure 2). The associated potential energy increase is then computed as

$$\Delta E_p(\Delta T) = \int_{h_m}^{0} \Big(\rho_f - \rho_i(z)\Big)\, g\, z\, dz, \tag{4}$$

where ρ_i is the initial unperturbed profile of density, g is the acceleration of gravity, z is ocean depth, ρ_f is the homogeneous final density profile. After the mixing, temperature T is assumed to be constant and equal to $SST + \Delta T$ within the mixed layer (Figure 2, top). Similarly, salinity S is assumed to be constant within the mixed layer and its value is computed from conservation of salt. Density ρ_f can then be obtained using these (T,S) values. $\Delta E_p(\Delta T)$ is finally computed from the density difference between the initial and final profiles, using equation (4). This computation of $\Delta E_p(\Delta T)$ hence only requires knowledge of the temperature and salinity profiles before the cyclone passage.

[21] In the following, we define the cooling inhibition (CI) as the cube root of the necessary potential energy to induce a 2°C SST cooling:

$$CI = [\Delta E_p(-2°\mathrm{C})]^{1/3}. \tag{5}$$

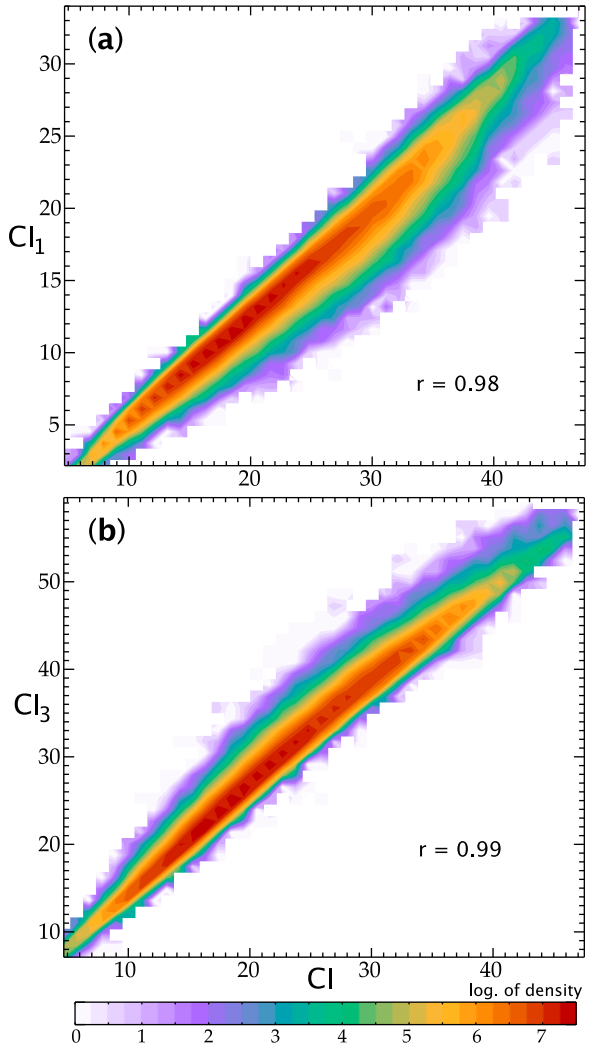

Figure 3. Probability density functions of (a) Cooling Inhibition calculated using a 1°C threshold (CI_1) versus a 2°C threshold (CI) and (b) Cooling Inhibition calculated using a 3°C threshold (CI_3) versus a 2°C threshold (CI). Correlations between these indices are, respectively, 0.98 and 0.99. Units are in $(J.m^{-2})^{1/3}$.

CI is defined as a cube root on the basis of the idealized analysis of section 3.1, which suggested that the cooling should scale as the cube root of a potential energy. The analysis preformed in Section 4 will provide further evidence of the relevance of this scaling. We compute cooling inhibition CI from a cooling of −2°C, a rather typical value under a tropical cyclone. The typical variations of CI over the cyclone-affected regions are anyway relatively insensitive to a choice of 1°C (CI_1), 2°C (CI) or 3°C (CI_3) (Figure 3): CI_1 and CI_3 are highly correlated (0.98 and 0.99) to CI.

[22] We call this index "Cooling Inhibition" (CI) because it measures the resistance of the ocean to surface cooling through mixing. CI is a useful metric to describe the oceanic inhibition to a wind-induced cooling because it integrates two relevant parameters for the cooling amplitude: the initial mixed layer depth and the strength of the stratification just below it. Indeed, the deeper the initial mixed layer, the more kinetic energy is required to produce mixing at its base. And the deeper the initial mixed layer, the greater the thermal capacity of the surface layer: for a given entrainment cooling, a thicker layer cools less. The stratification at the base of the mixed layer is another relevant parameter because it sets the temperature of water that can be entrained into the mixed layer. Figure 4a shows that CI accounts for both these parameters: it increases with the mixed layer depth (h_i) and decreases with the stratification at its base (N). Largest CI are only found when the mixed layer is deep and the stratification at its base is weak. We will show in the following that CI accurately describes the ocean propensity to mitigate

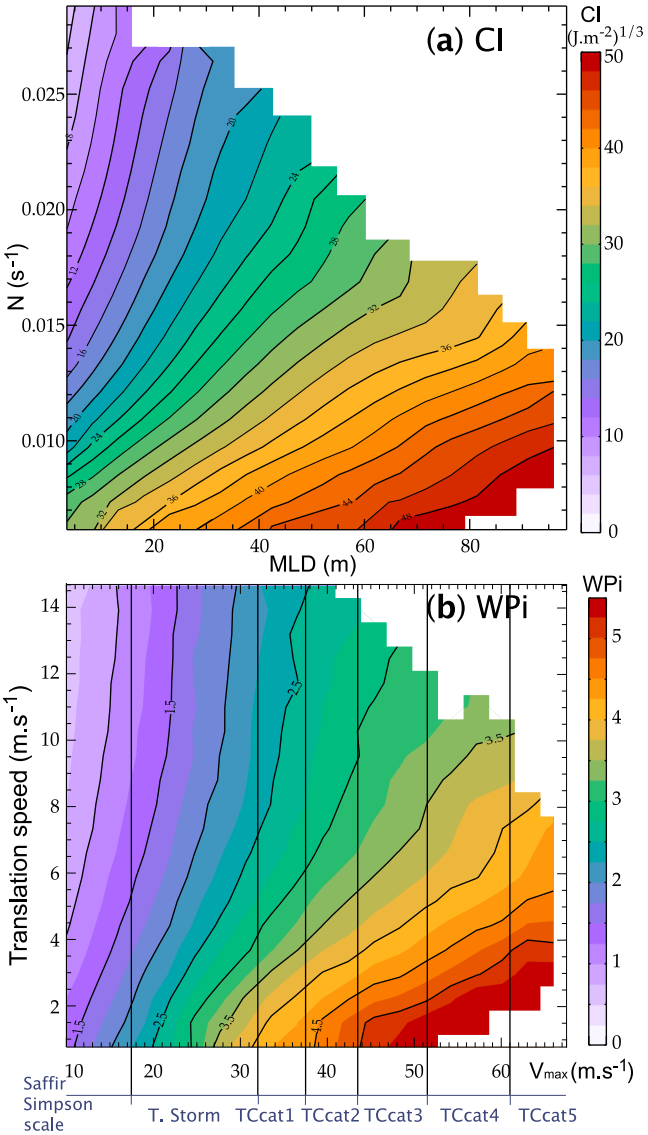

Figure 4. (a) Average CI values as a function of the mixed layer depth (MLD) and the stratification at its base (N) evaluated as $N^2 = \alpha g \frac{T_{ML}-2°C}{h_2-h_i}$, where h_2 is the depth of the isotherm "T_{ML}-2°C" and h_i the mixed layer depth. (b) Average $WPi = [PD/PD_0]^{1/3}$ as a function of the maximum 10-min sustained wind (V_{max}) and TC translation speed. For representativeness, the mean is limited to regions with 6 samples or more. Saffir–Simpson tropical cyclone scale is reminded for reference.

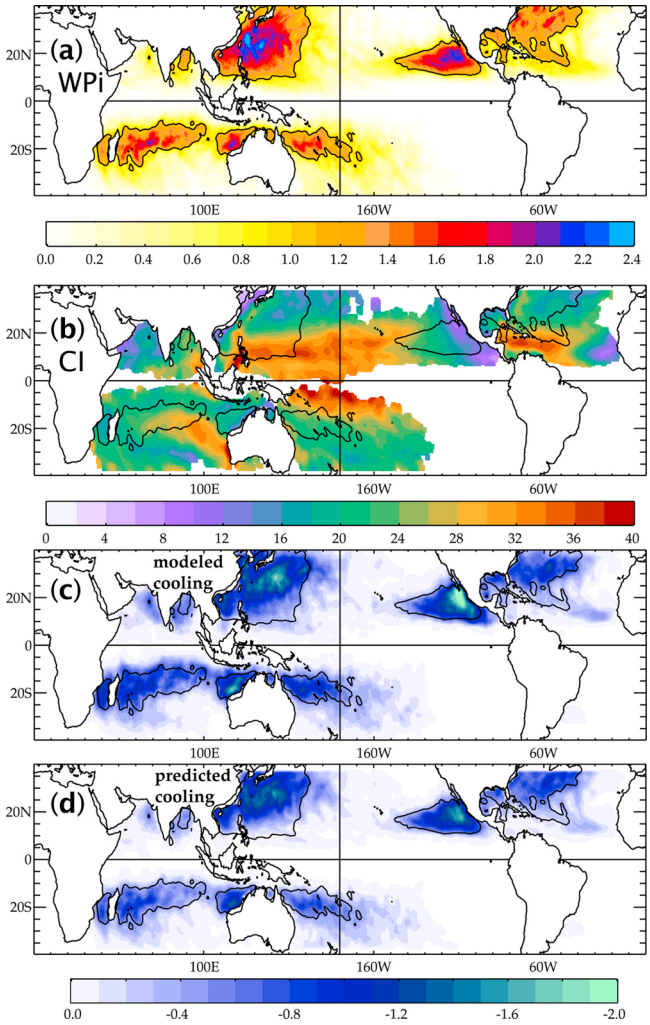

Figure 5. Maps over 1978–2007 of average (a) wind power index, (b) CI (in $(J.m^{-2})^{1/3}$), (c) TC-induced cooling in the ocean model and (d) cooling predicted with the bivariate fit on *WPi* and CI (in °C). For each cyclonic season, a map is obtained by first recording the integrated-*WPi*, CI or ΔT_{CW} within 200 km of each TC position and averaging for all TCs of the season. Figure 5 shows the 30-years average of these seasonal maps. Isoline "*WPi* = 1" is repeated over each panel for reference.

the SST response to a cyclone. In the rest of the paper, we compute CI in our simulation based on the pre-storm ocean column density (averaged over 10 to 3 days before TC passage, and within 200 km from the TC track position). Figure 5b illustrates the average CI value under all TCs track in our simulation, for all pre-cyclone oceanic profiles during 1978–2007 (this figure does not strongly differ from the figure of the CI computed from the oceanic climatological state during the cyclonic season in *Vincent et al.* [2012, Figure 3e]). This map partially reflects the depth of the thermocline (larger energy is required to bring cold water parcels to the surface when the thermocline is deep), with large CI values in the western Pacific warm Pool or in the Northwestern Tropical Atlantic. CI does not only reflect thermal stratification, but also haline stratification: CI is larger in the Bay of Bengal than in the Arabian Sea, partly due to the very strong river runoffs and resulting haline stratification in the Bay, that prevents vertical mixing [*Sengupta et al.*, 2008; M. Neetu et al., Influence of upper ocean stratification on tropical cyclones-induced surface cooling in the Bay of Bengal, unpublished manuscript, 2012].

3.3. A Metric of the Atmospheric Control of TC-Induced Cooling

[23] The kinetic energy transferred by the storm to the upper ocean can be computed from the work W of surface wind stress on the ocean $W = \int_{t_o}^{t_c} \boldsymbol{\tau} \cdot \mathbf{u}_{oce}\, dt$ where $\boldsymbol{\tau}$ is the surface wind stress, $\mathbf{u}_{oce}$ the surface ocean current, t_o the time when the storm starts influencing a certain point and t_c the current time. In this paper, t_o is set to day −3 (3 days before a TC reaches a given ocean point). Taking t_o equal to day −5 or day −10 however yields very similar results, as most of the energy transferred to the ocean occurs within a couple of days before and after the cyclone reaches a given location. t_c is taken as day +3 to integrate the wind-forcing over the full period during which the TC influences the ocean column and relate it to the cooling occurring in the wake of the TC.

[24] While W can easily be calculated in our simulation, it is not available in observations due to the lack of reliable high-frequency estimates of observed surface currents. A more easily computable quantity is the power dissipated by friction at the air-sea interface. *Bister and Emanuel* [1998] showed that, in a hurricane, dissipation occurs mostly in the atmospheric surface layer, with a dissipation rate per unit area, D, given by: $D = \rho C_D |V|^3$. In our simulation, we find that the time integral of this dissipation (Power Dissipation (PD)) [*Emanuel*, 2005] is highly related to W (correlation of 0.9) as shown on Figure 6. It can hence be used as a proxy to estimate the kinetic energy transferred to the ocean W. Because it is more easily estimated from observations and

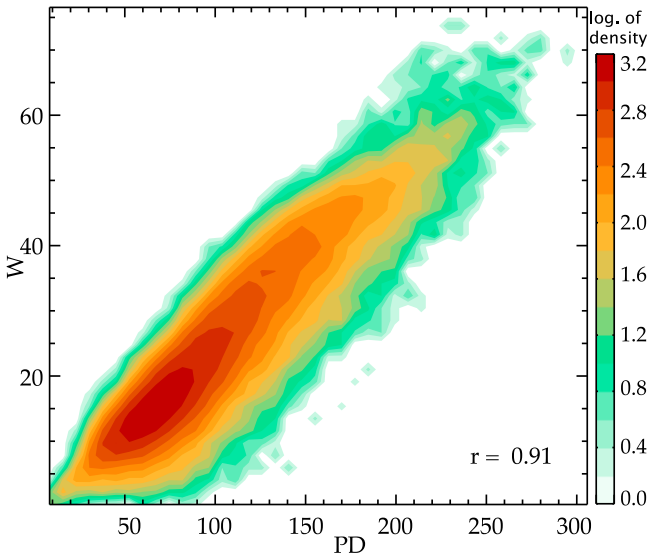

Figure 6. Probability density function of the wind work on surface currents (W) versus the Power Dissipated (PD) averaged within 200 km of each TC track position. Correlation between these two quantities is 0.91. Units are in $(J.m^{-2})^{1/3}$.

can be used for future studies, we will hereafter use *PD*, calculated at every point along cyclone tracks as

$$PD = \int_{t_o}^{t_c} \rho\, C_D |\mathbf{V}|^3\, dt, \quad (6)$$

where $|\mathbf{V}|$ is the local magnitude of surface wind, C_D the dimensionless surface drag coefficient [*Large and Yeager*, 2009] and ρ the surface air density.

[25] The cooling amplitude can be related to TC wind-forcing by the very crude assumption that the kinetic energy input W (approximated by PD) linearly relates to the potential energy increase in the ocean. Using the idealized approach of section 3.1 and equation (3), this leads to a ΔT that should be proportional to $W^{1/3}$ for cases where the initial mixed layer is shallow (~80% of the TC cases). It is however far from being obvious that the fraction of kinetic energy transformed into potential energy is constant as it is likely to depend for instance on the relative ML depth and wind-induced mixing depth. A similar dependence of ΔT to $W^{1/3}$ can also be derived using a different framework that directly relates surface cooling to wind-forcing such as the one developed in the appendix of *Korty et al.* [2008]. Using this framework based on the *Price* [1979] assumption that the bulk Richardson number remains constant during TC mixing, one can demonstrate that the temperature change scales as the cube root of the wind power input for shallow MLDs. This provides further theoretical justification for the choice of the scaling for the index proposed below.

[26] We hence define a dimensionless "wind power index" as

$$WPi = [PD/PD_0]^{1/3}, \quad (7)$$

where $PD_0 = \int_{t_o}^{t_c} \rho\, C_D |\mathbf{V}_0|^3\, dt$ is a normalization constant corresponding to a typical weak storm with a translation speed of 7 m.s^{-1} (25 km.h^{-1}) and maximum 10-min averaged wind speed of 15 m.s^{-1} (the wind speed defining a Tropical Depression: the weakest cyclonic system classified). *PD* is computed using the same choices for t_0 and t_c as for *W*. The almost linear relationship between average ΔT and WP_i (that will be shown later in the paper) illustrates the first order validity of this simple approach for the scaling definition.

[27] Previous studies have underlined that not only cyclone intensity, but also translation speed influences the amplitude of the cold wake, slower cyclones being associated with intense cooling [*Greatbatch*, 1984; *Lloyd and Vecchi*, 2011]. Figure 4b shows that *WPi* gathers information about these two factors. *WPi* increases (decreases) monotonically with storm intensity (translation speed), and reaches its highest values (~5) for TCs that are both strong and slow (Category 4 or more on the Saffir-Simpson scale and translation speed <4 m/s). Bigger storms are also characterized by a longer influence of strong wind-forcing at a given point; WP_i also naturally integrates the storm size effect.

[28] Figure 5a shows the average *WPi* by basin. It underlines familiar regions of TC occurrence. Most powerful TCs occur in the northeast and northwest tropical Pacific. There is also a high averaged wind power North of Australia (both on the Indian ocean and Pacific sides), and in the Southwestern Indian Ocean. The Caribbean and Northern Indian Ocean display the weakest averaged wind power. In the following section, we will discuss the upper-ocean cooling, in response to this forcing.

4. Dependence of the Cold Wake Magnitude to TC and Ocean Characteristics

[29] Using the two metrics described above, the following section quantifies the dependency of the cooling amplitude on the oceanic background state. The improvement brought by including this oceanic metric in the CW intensity hindcast is then assessed. The efficiency of CI against other proposed oceanic metrics is finally discussed.

4.1. Surface Cooling as a Function of *WPi* and CI

[30] The average cooling under TCs largely reflects the spatial distribution of *WPi* (Figures 5a and 5c), but a closer inspection reveals that maximum cooling are in general not collocated with maximum *WPi*. For example, the maximum cooling occurs poleward of the maximum energy input in the northwestern Pacific as less energy is required to cool the ocean there (low CI values; Figure 5b). The maximum cooling intensity in the Southwestern Indian Ocean is similarly shifted to the west (e.g., into the Mozambique channel) of the *WPi* maximum. The spatial distribution of the average TC cooling (Figure 5c) is hence a consensus between the energy input (Figure 5a) and the cooling inhibition by ocean stratification (Figure 5b).

[31] Figure 7a shows a probability distribution of the cooling as a function of *WPi*. The mean cooling increases with *WPi*, as suggested by the idealized approach in section 3. This increase is almost linear for *WPi* <4, justifying a posteriori the relevance of *WPi* formulation and scaling to estimate the cold wake amplitude. The slope of ΔT versus *WPi* however increases for *WPi* larger than 4. This nonlinearity probably arises from the fact that Figure 7 accounts for all simulated cooling, including cases of deep initial mixed layer (~20% of the cases) for which the scaling between ΔT and ΔE_p (and hence PD) is different (see section A1). In addition, it is likely that the ratio of potential energy increase (ΔE_p) to the wind energy transferred to the ocean (*W*) depends on the initial ML depth relative to the TC-induced mixing length, thus being dependent on *W* itself. The simple cube root scaling used for the *WPi* definition is thus a first order approach that may be further improved. The proposed *WPi* variable however fulfills our main objective, which was to define a metric that condenses the main TC parameters that affect the cooling into a single explanative variable, from which ΔT is a monotonically increasing function. This is not the case for the widely used V_{max} (TC maximum winds) variable [*Lloyd and Vecchi*, 2011]). Although the mean cooling increases with *WPi* (Figure 7a), there is a large scatter of the cooling amplitude around this mean value. For a given wind energy, the cooling of the 5th and 95th percentile of events differs by one order of magnitude. For instance, a *WPi* of 4 results in a cooling ranging from 0.5°C to 5°C. We will show below that this scatter of the cooling magnitude can be largely explained by the influence of the oceanic background state, as measured by the CI parameter.

[32] Figure 8a shows that the average cooling increases as a function of *WPi* and decreases as a function of *CI*. Very large cooling (up to 5°C) only occur when powerful TCs (*WPi* > 4) travel over a very stratified upper ocean (low CI).

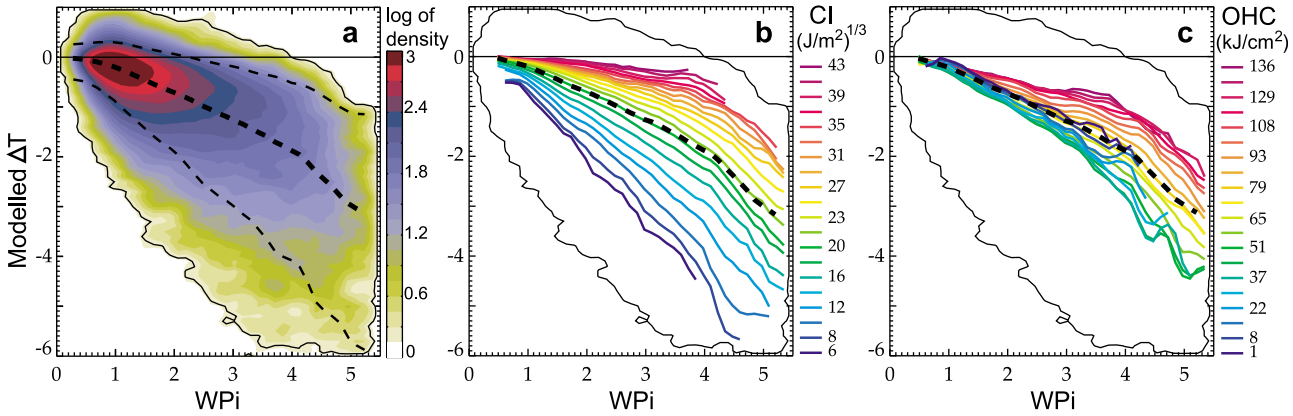

Figure 7. (a) Probability density function of storm-induced cooling ΔT versus wind power index *WPi*. The thick dashed line indicates the average cooling as a function of *WPi* while the thin dashed lines represent the highest and lowest 5% of the distribution. (b) Average cooling as a function of *WPi* for 20 regularly spaced values of Cooling Inhibition (CI). (c) Same as Figure 7b but for the Ocean Heat Content (OHC). Contour of 0.1 probability density isoline from Figure 7a is reported on Figures 7b and 7c (thin plain line) as well as the average cooling as a function of *WPi* (dashed line).

Figure 7b further displays the average cooling as a function of *WPi* binned by *CI* values (the dark blue curves corresponding to low values of *CI* and the purple curves to high values of *CI*). Taking *CI* into account allows one to explain the wide range of possible TC cooling amplitudes for a given wind power input (Figure 7b). For a large *CI*, the cooling is about an order of magnitude smaller than for a weak *CI*. For example, the average cooling for a *CI* of ~40 $(J.m^{-2})^{1/3}$ never exceeds 0.5°C, while it can reach up to 5°C for a *CI* of ~10 $(J.m^{-2})^{1/3}$. This demonstrates that oceanic stratification is a major factor controlling the SST response to a TC.

[33] This control of the surface cooling magnitude by the oceanic background state is further quantified by comparing cooling prediction skills of hindcasts based on the atmospheric metric alone (*WPi*) or on *WPi* along with *CI*. Simple bivariate statistical models of ΔT are constructed based on *WPi* and *CI* from a least squares fit of the surface $\Delta T = f(WPi, CI)$ of Figure 8a in the form

$$\Delta T_{predicted} = c_0 + c_1 \times WPi + c_2 \times CI + c_3 \times WPi \times CI. \quad (8)$$

[34] The performance of this model can be qualitatively assessed by comparing the spatial distribution of the average predicted cooling against the actually simulated cooling (Figures 5c and 5d). Despite an underestimation of the extrema, Figure 5d shows that the bivariate model is able to describe the average cooling distribution from *CI* and *WPi*.

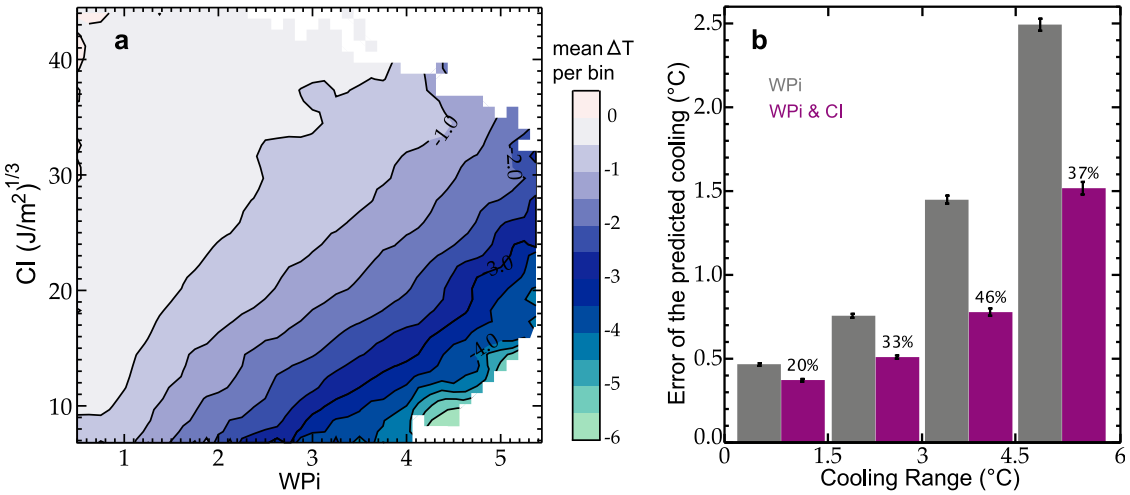

Figure 8. (a) Average cooling for any couple of WPI and CI. The mean cooling is shown here for 40 regularly spaced bins of *WPi* and 40 bins of CI. For representativeness, the mean is limited to regions with 6 samples or more. (b) Mean absolute error of a linear prediction of the simulated cooling using *WPi* as a single predictor (gray) and *WPi* and CI as a couple of predictors (purple). The percentage of improvement with respect to using *WPi* alone is indicated over each bar. Error bars give the 90% confidence interval estimated from a bootstrap technique (as explained in section A2).

Table 1. Percentage of Improvement in The Mean Absolute Error of the Predicted Cooling Brought by the Use of Both CI and *WPi* With Respect to *WPi* Alone[a]

Cooling Range (°C)	MOD ΔT_{CW}	MOD ΔT_{eye}	OBS ΔT_{CW}
0–1.5	20	13	9
1.5–3	33	35	16
3–4.5	46	31	16
4.5–6	37	18	14

[a]MOD ΔT_{CW}, MOD ΔT_{eye}, OBS ΔT_{CW}, respectively, corresponds to the hindcast improvement for modeled wake cooling (as in Figure 8b), the modeled inner-core cooling and the observed wake cooling from TMI-AMSRe. For the hindcast of the inner-core cooling (ΔT_{eye}), end time for integration (t_e) is taken as day +0 in the *WPi* calculation.

More quantitatively, using both *CI* and *WPi* clearly reduces the error of the predicted cooling compared to using *WPi* alone. Using *WPi* alone yields a ∼50% relative error on the cooling prediction for all range of cooling magnitude. Using *WPi* and CI allows to reduce this relative error to an average of ∼30%. For instance, while the prediction error is 1.4°C for a 3°C cooling using *WPi* alone, this error is reduced to 0.8°C when using both CI and *WPi.* The improvement of the relative error is larger for the most intense cooling, ranging from 33% to 46% for cooling between 1.5°C and 6°C (Figure 8b). The relative improvement brought by the inclusion of CI is weaker for weak cooling (20%). This may be related to the larger contribution of surface heat fluxes to the total cooling for weakest cooling [*Vincent et al.*, 2012] that are not expected to be sensitive to sub-surface stratification.

[35] The above results discuss the modeled cyclone cold wake ΔT_{CW} (i.e., cooling after the cyclone passage). The relevant parameter to investigate ocean influence on TC intensity is not cooling in the cyclone wake ΔT_{CW}, but inner-core cooling ΔT_{eye} (cooling under the storm eye) [*Cione and Uhlhorn*, 2003; *Schade*, 2000] for which satellite observations are not reliable. In our model, however, we can estimate the ability of the various metrics to predict the inner-core cooling ΔT_{eye}. Inner-core cooling and cold wake are in fact highly correlated in our simulation (correlation coefficient of 0.8, as discussed by *Vincent et al.* [2012]). *CI* also improves the predictive skills of *WPi* for the inner-core cooling, most substantially for intermediate cooling intensities (improvement of more than 30% for cooling between 1.5°C and 4.5°C) (Table 1). Finally, using *CI* (calculated from model outputs) also improves estimates of the *observed* ΔT_{CW} cooling (from TMI-AMSRE) by up to 16% compared to atmospheric information alone (Table 1). This weaker skill compared to the modeled cooling prediction is easily understandable. Our model without data assimilation does not realistically simulate locations of oceanic mesoscale structures, and suffers from systematic bias in some regions. The improvement above would hence arguably be better with a model properly constrained by observations through data assimilation [e.g., *Drevillon et al.*, 2008]. This result however suggests that *CI* not only allows predicting the TC-cooling in the model world, but is also helpful to improve the prediction of observed cooling under TCs.

4.2. Comparison of CI to Other Metrics

[36] This paper proposes a physically based metric to account for the influence of the upper ocean stratification onto TC-induced cooling. Aside from OHC, recent papers have proposed other alternatives to quantify the effect of oceanic background state on TCs. These alternatives include T100 (temperature averaged in the upper 100 m, the typical mixing depth of a strong TC) [*Price*, 2009] the Interacting Tropical Cyclone Heat Content (ITCHC, the heat content in the mixed layer) [*Buarque et al.*, 2009], or the depth of the mixed layer temperature isotherm minus 2°C, hereafter h_2 [*Lloyd and Vecchi*, 2011]. In this subsection, we gauge all these metrics by their ability to estimate the TC-induced cooling globally, over the last 30 years.

[37] OHC is the most popular index of oceanic control of air-sea interactions below cyclones. However, unlike *CI*, OHC only explains a small fraction of the wide range in TC-induced cooling amplitudes for a given wind power (Figure 7c): the lowest values of OHC are shown to be unable to describe the most intense cooling events, in contrast to *CI.* The relation between OHC and the cooling is also not monotonous: for weak OHC, the cooling first increases and then decreases with OHC. A measure of the thermal energy of the upper ocean hence only partially describes the CW dependence to ocean characteristics.

[38] A more quantitative comparison is provided by comparing the improvement brought by each ocean metric to hindcast the cooling magnitude using the bivariate model described above. Metrics based on a thermal energy definition (OHC, ITCHC, T100) do not perform as well (only up to 20% improvement) compared to CI and h_2. These two variables both induce up to ∼45% improvement to the predicted cooling. They display a similar performance, except for the weakest cooling range (<1.5°C) for which CI allows a significantly greater improvement. The modest performance of the measures based on thermal energy (OHC, ITCHC, T100) is related to the use of the absolute temperature in those metrics, which is useful to predict the absolute temperature after the cyclone, but not the cooling magnitude. Modifying T100 by subtracting the SST to it (*SST-T100*) indeed results in a considerable improvement of the prediction skills (Figure 9), with the largest improvement (∼43%) for the strongest cooling range (>4.5°C). A measure such as *SST-T100* is indeed appropriate to describe a surface cooling associated to a deep mixing (100 m is a typical mixing depth for a category 3 hurricane [*Price*, 2009]).

[39] While not explicitly taking physical processes of the cooling into account, h_2 performs as well as *CI.* This metric is highly correlated to *CI* (correlation coefficient of 0.94) and basically measures the same information as *CI* does: namely the depth of the ML and the importance of the temperature stratification at its base. h_2 can actually be expressed in a similar way as *CI* if we assume that density is proportional to temperature. In the simple case where $h_i = 0$ (presented in section 3.1), h_2 can be written as $h_2 = \left(\frac{3}{2}\frac{\Delta E_p}{\rho_0 N^2}\right)^{1/3}$, hence h_2 is expected to scale as *CI* (see Annex A1 for the calculation). In our global analysis, h_2 skills are very similar to *CI* and its definition is somehow simpler. However, the h_2 definition does not account for the effect of salinity on stratification. This effect can be important in some regions, for example in the Bay of Bengal where haline stratification can reduce the amplitude of TC-induced cooling after the monsoon [*Sengupta et al.*, 2008; Neetu et al., unpublished manuscript, 2012]. *CI* brings a larger improvement than h_2 for cooling predictions over the Bay of Bengal (Table 2). This is an

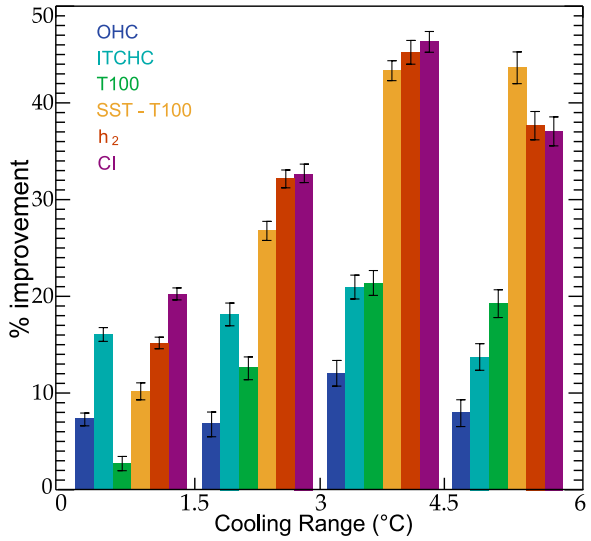

Figure 9. Percentage of improvement in the mean absolute error of the predicted cooling brought by the inclusion of various ocean metric in addition to *WPi* in the predictors (as in Figure 8b): OHC (dark blue), ITCHC (light blue), T100 (green), SST-T100 (yellow), h_2 (red), and CI (purple). Error bars give the 90% confidence interval estimated from a bootstrap technique (as explained in section A2).

illustration that, although h_2 is generally a good indicator of the cooling, the integration of salinity effects into the CI index makes it appropriate for a wider range of oceanic conditions.

5. Conclusion

[40] Sea surface temperature (SST) influences tropical cyclones (TCs) intensity through two mechanisms: (1) ambient SST that sets the maximum potential intensity for TCs and (2) the negative feedback associated with the cooling under the TC eye. TCs intensity is more sensitive to the feedback associated with the cooling than to the ambient SST [*Schade*, 2000]. *Lloyd and Vecchi* [2011] further demonstrated that the TC intensity evolution is linked to the observed cooling magnitude in the wake of TCs, and suggested that the ocean sub-surface temperature stratification is a key parameter in controlling the TC intensity evolution through its modulation of the SST feedback.

[41] This paper provides a comprehensive and global quantification of the sensitivity of TC-induced cooling amplitude to pre-storm ocean state. In order to overcome limited availability of ocean in situ data below tropical cyclones, we use an ocean general circulation model experiment that realistically samples the ocean response to more than 3,000 TCs. As cooling largely results from mixing, i.e., a conversion of mechanical into potential energy, we propose to describe the ocean effect on the TC-induced cooling by two metrics: a wind power index (*WPi*) and a Cooling Inhibition index (CI). *WPi* is a proxy of the kinetic energy provided to the ocean by a TC, which triggers upper-ocean mixing. It integrates the effects of various TC parameters (maximum winds, translation speed, size) that affect the TC-induced cooling. CI is a measure of the input of potential energy required to cool the surface ocean by 2°C through vertical mixing. It thus accounts for the pre-storm upper ocean stratification and its resistance to surface cooling via mixing.

[42] We show that these two simple metrics are relevant to explain the wide TC-induced cooling amplitude distribution. While average cooling increases with *WPi*, a given *WPi* (i.e., a given kinetic energy deposit in the ocean) can be associated to a wide range of cooling. Our results demonstrate that contrasts in upper ocean stratification, as measured by CI, explain most of this range. Ocean pre-storm stratification modulates the cooling magnitude by up to an order of magnitude for a given wind energy input. For example, for high *WPi*, the cooling amplitude varies from 0.5°C to 5°C depending on CI (a high CI resulting in a small cooling). Upper ocean stratification is thus a key factor for the CW magnitude.

[43] We further show that using CI in addition to *WPi* improves statistical hindcasts of the cold wake amplitude by ~40% (for cooling larger than 1.5°C). Previously proposed metrics that are based on a fixed threshold and/or absolute temperature (i.e., OHC, T100, ITCHC) do not predict accurately the CW magnitude. In contrast, metrics that account for both mixed layer depth and the steepness of the stratification at its base (e.g., h_2, SST-T100) display comparable hindcast skills to CI. The main interest of CI is however to rely on the physical mechanism responsible for the oceanic control of the CW namely the amount of potential energy required to yield a given surface cooling. Still, our results suggest that CI is a better alternative than previously proposed metrics of cyclone-ocean interactions in regions where haline stratification plays an important role in controlling the surface cooling, like the Bay of Bengal [*Sengupta et al.*, 2008; Neetu et al., unpublished manuscript, 2012].

[44] We think that this work may have practical consequences for cyclone intensity forecasts. While OHC only brought modest ~5% improvement to TC intensity statistical forecast schemes [*DeMaria et al.*, 2005; *Mainelli et al.*, 2008], a metric like CI, which properly captures the ocean propensity to modulate TC-induced surface cooling (and hence the storm growth rate), could be tested in TC intensity forecast schemes. CI calculation requires both salinity and temperature profiles in front of the storm track and is thus harder to compute operationally than metrics based on temperature profile alone. Temperature and salinity data are provided by ARGO measurements, but their spatial and temporal coverage is not sufficient to sample all pre-cyclones oceanic conditions. Even though salinity stratification partly controls the surface cooling in some regions such as the Bay of Bengal, a first approach could be to calculate CI

Table 2. Percentage of Improvement in the Mean Absolute Error of the Predicted Cooling Brought by the Inclusion of Various Ocean Metrics in Addition to *WPi* for the Bay of Bengal

Cooling Range (°C)	Percent Improvement for Bay of Bengal MOD ΔT_{CW}					
	OHC	ITCHC	T100	SST-T100	h_2	CI
0–1	3	14	4	10	12	20
1–2	2	6	4	20	23	32
>2	10	8	10	26	37	45

with temperature stratification only, which can be reconstructed from altimetry measurements in the same manner as OHC [*Shay et al.*, 2000]. Alternatively, CI could also be computed from currently available operational oceanography products constrained by oceanic observations [e.g., *Drevillon et al.*, 2008].

[45] Although CI rather accurately captures the upper ocean propensity to modulate the amplitude of TC-induced cooling, we believe that our approach can be further improved. The scaling used to define both CI and *WPi* are based on rather crude assumptions. For instance, we hypothesized a linear relationship between the energy input from the wind and the potential energy increase in the ocean to derive the cube root scaling of *WPi.* It is however likely that the fraction of kinetic energy transformed into potential energy depends on oceanic parameters such as the mixed layer depth and the wind-induced mixing depth. A careful investigation of the mechanical energy budget under TCs is required to shed light on the energy transfer from surface winds to surface currents and quantify the respective amount of energy that is locally converted to potential energy or radiated away in the form of internal waves.

[46] Our aim in this paper was to quantify the influence of the oceanic stratification on TC-induced cooling globally, not to include all the physically relevant processes into an analytic prediction of the TC-induced cooling. In a way similar to *Schade and Emanuel* [1999], a potential route for a more accurate prediction of TC-induced cooling would be to include other relevant parameters of the TC-ocean interaction. An inherent limitation to the CI definition is indeed to only account for the TC-induced cooling driven by penetrative vertical mixing. Mixing generally dominates surface cooling for moderate to high wind power but cooling by air-sea fluxes also plays a significant role for weak TCs [*Vincent et al.*, 2012]. The surface cooling also depends on the amplitude of the upwelling induced by the TC that alters the thermal stratification [*Yablonsky and Ginis*, 2009]. Accounting for these processes (surface fluxes and advection) may further improve the forecast skills of the TC-induced cooling. In addition, while our results allow us to illustrate the strong impact of the oceanic background conditions on the amplitude of the TC-induced surface cooling, we did not directly assess the influence of the oceanic background conditions of the cyclone intensification itself. As demonstrated by *Schade and Emanuel* [1999], the effect of a given cooling on a TC also depends on characteristics of the TC itself such as its intensity and translation speed. A statistical forecasting technique of TC intensity including the parameters proposed in the present study should allow to address this issue.

[47] Finally, some studies suggest that ocean eddies [e.g., *Jacob and Shay*, 2003] or low frequency climate variations [e.g., *Xie et al.*, 2002] impact tropical cyclones activity through modification of the TC-induced cooling magnitude. Our approach offers potential for quantifying the extent to which ocean stratification changes linked to natural ocean variability can mitigate cyclone intensity. Changes in the atmospheric background state driven by anthropogenic forcing could also alter cyclone distributions in present and future climate [*Knutson et al.*, 2008]. Our approach may also allow to estimate the potential influence of upper-ocean stratification changes driven by climate change on future TCs cooling amplitude and ultimately on TCs intensification. In contrast to OHC, T100 or ITCHC, CI is suited to perform such an investigation, as its definition does neither depend on absolute temperature nor on fixed thresholds representative of the present-day climate [*Royer et al.*, 1998].

Appendix A

A1. Idealized Framework to Illustrate Surface Cooling Scaling

[48] The purpose of this appendix is to develop the approach in section 3.1 to the more realistic case where a mixed layer is present (i.e., the ocean is not linearly stratified all the way up to the surface). Depending on the mixed layer depth, two forms of solutions can be derived for the scaling between surface cooling and potential energy input associated to vertical mixing.

[49] Let us consider an ocean with constant stratification N^2 under a ML of initial depth h_i as illustrated on Figure A1a, and a linear equation of state with density depending on temperature only: $\rho(z) = \rho_0(1 - \alpha\, T(z))$. The temperature profile is $T(z) = \begin{cases} T_i & ,z > -h_i \\ T_i + \Gamma(z + h_i) & ,z < -h_i \end{cases}$ with $N^2 = -\frac{g}{\rho_0}\frac{\partial \rho}{\partial z} = \alpha g \frac{\partial T}{\partial z} = \alpha g \Gamma$. α is the coefficient for thermal expansion of seawater, ρ_0 is a reference density and Γ is the temperature gradient under the ML.

[50] Let us now assume that after the 'passage of the cyclone;' the surface layer has been homogeneously mixed down to the depth h_m, at the temperature T_f (Figure A1a).

[51] Conservation of heat yields an equation linking h_m with the surface cooling $\Delta T = T_f - T_i$

$$\int_{-h_m}^{0} \rho_o C_P (T_f - T_i(z)) dz = 0. \tag{A1}$$

Assuming constant C_P and ρ_o ($\rho \approx \rho_o$ at the first order in $\rho \times T$) and $h_m \neq 0$ yields:

$$h_m^2 - 2\, h_2\, h_m + h_i^2 = 0, \tag{A2}$$

where $h_2 = h_i - \frac{\alpha g}{N^2}\Delta T$ (as defined on Figure A1a is the variable discussed by *Lloyd and Vecchi* [2011] when $\Delta T = -2°\mathrm{C}$).

[52] The potential energy difference between the initial and final profile is

$$\Delta E_p = \int_{-h_m}^{0} \left(\rho_f - \rho_i\right) g\, z\, dz, \tag{A3}$$

providing an equation linking h_m, ΔT and ΔE_p

$$h_m^3 - \frac{3}{2} h_2\, h_m^2 + \frac{h_i^3}{2} = H^3, \tag{A4}$$

with $H \equiv \left(\frac{3\Delta E_p}{\rho_0 N^2}\right)^{1/3}$. H can be seen as a characteristic mixing length associated to a potential energy input ΔE_p.

[53] From (A2) and (A4), it is possible to derive the dependence of the surface cooling ΔT to the potential

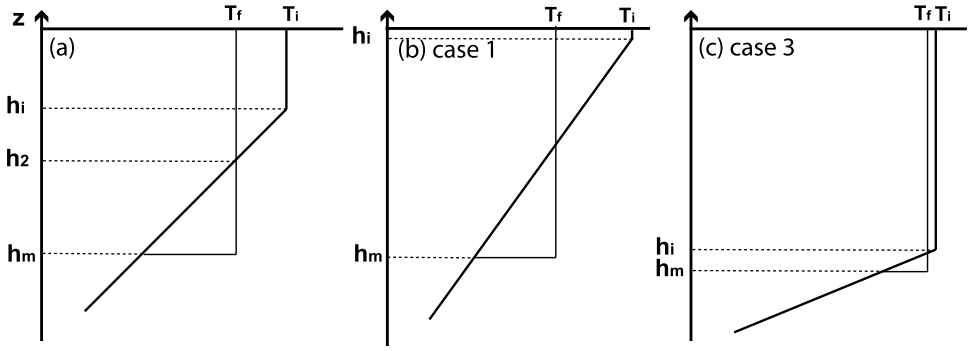

Figure A1. Temperature profile (a) with "normal" ML, (b) with shallow ML and (c) with "deep" ML corresponding to the different cases used in the calculation of the scaling between the surface cooling and the associated potential energy increase of the water column.

energy increase of the water column ΔE_p. Substituting (A2) into (A4) yields

$$h_m^3 - 3h_i^2 h_m + 2(h_i^3 - 2H^3) = 0 \qquad \text{(A5)}$$

that can be set in the reduced Cardan's form $h_m^3 + 3ph_m + 2q = 0$ (with $p = -h_i^2$ and $q = h_i^3 - 2H^3$).

[54] The resolution of (A5) is conditioned to the sign of $\Lambda \equiv p^3 + q^2$ and the different cases lead to different scaling of the surface cooling versus the energy input:

[55] *Case 1.* If $\Lambda > 0 \Leftrightarrow h_i < H$ (i.e., the initial MLD is shallower than the typical mixing length), then there is one solution $h_m = \sqrt[3]{-q - \sqrt{\Lambda}} + \sqrt[3]{-q + \sqrt{\Lambda}}$. In the limit $h_i \to 0$, $h_m \approx 4^{1/3} H$ and $\Delta T \approx -\frac{1}{\alpha g}\left(\frac{3N^4}{2\rho_0}\Delta E_p\right)^{1/3}$; in this case (presented in the part 3.1 of the paper), there is a cube root scaling between the surface cooling and the potential energy increase.

[56] *Case 2.* If $\Lambda = 0 \Leftrightarrow h_i = H$ (i.e., the initial MLD equals the typical mixing length), there is one positive solution for h_m: $h_m = 2h_i$, and $\Delta T = \frac{-N^2 h_i}{4\alpha g} = \frac{-1}{4\alpha g}\left(\frac{3N^4}{\rho_0}\Delta E_p\right)^{1/3}$. We note that this intermediate case occurs when the final mixed layer depth is twice the initial one.

[57] *Case 3.* If $\Lambda < 0 \Leftrightarrow h_i > H$ (i.e., the initial MLD is deeper than the typical mixing length) there are 3 solutions for h_m but only one real positive: $h_m = 2h_i \cos\left(\frac{1}{3}\arccos\left(\frac{2H^3}{h_i^3} - 1\right)\right)$. (1) In the limit when $h_i = H$, $h_m = 2h_i$, the cube root scaling still applies as in case 2. (2) In the limit when $h_i \gg H$, then $h_m \approx h_i\left(1 + 2\sqrt{\frac{H^3}{3h_i^3}}\right)$ and $\Delta T \approx -\frac{2}{\alpha g \rho_0 h_i^2}\Delta E_p$; in this case the scaling between surface cooling and energy input is linear.

[58] Figure A2 illustrates the frequency with which case 1 and case 3 occur in our numerical experiment. Case 1 appears to occur more often: 80% of the time under systems of tropical cyclones strength. One would remark that the upwelling induced by TCs under their track further participates in reducing the mixed layer depth, favoring the occurrence of case 1 scaling. Based on this analysis, we chose to use a cube root scaling in the definition of the cooling inhibition index although it may not reflect the scaling for all cases.

A2. Confidence Interval for Figures 8b and 9

[59] The confidence interval for the Mean Absolute Error of predicted TC-induced cooling is estimated using a bootstrap technique (Figures 8b and 9). We consider three distinct ranges of cooling amplitude ([0,2], [2,4], [4,6]°C). In each range, the N observations of the absolute difference

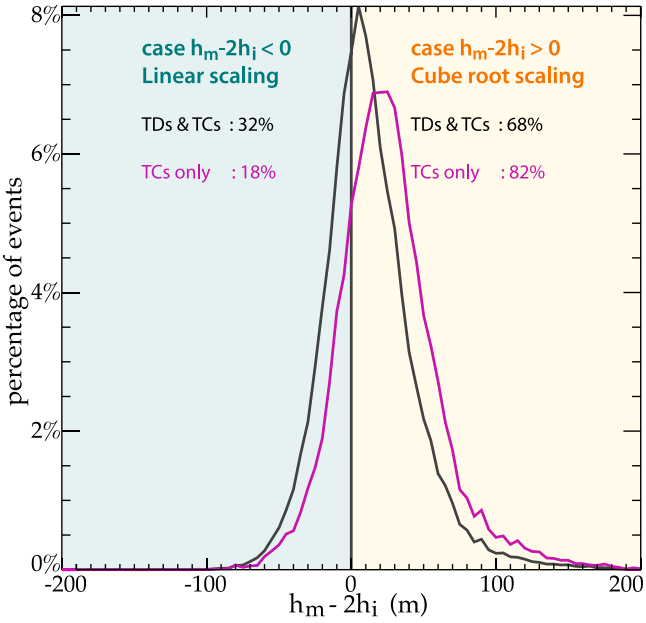

Figure A2. Histogram of the percentage of TC events associated to h_m-$2h_i$ values; according to the resolution of equation (A5), surface cooling scales linearly with ΔE_p when h_m-$2h_i \ll 0$ and scales as the cube root of ΔE_p when h_m-$2h_i > 0$. h_i is the MLD measured one week before TC passage and averaged within 200 km of each TC track position and h_m (the mixing depth) is calculated to obtain the modeled surface cooling by a heat conserving mixing. The black curve for both Tropical Depressions (TDs) and TCs shows the histogram for all systems with 10-min averaged winds greater than 15 m/s, the purple curve for TCs only shows systems with winds greater than 33 m/s.

between the predicted cooling $\Delta T_{predicted}$ and the actual cooling ΔT are called events. We randomly select N events from the total number of events in each range. Overlapping selection is allowed, meaning that one event can be selected more than once. From the selected N events, we calculate the average absolute error. By repeating this process 1,000 times, we obtain 1,000 values for the MAE. The upper and lower limit of each error bar (in Figures 8b and 9) represents the 5% and 95% percentile of the probability distribution function. If the MAE value using *WPi* and *CI* lies outside the error bar of the *WPi* alone, the improvement is significant at the 90% confidence level.

[60] **Acknowledgments.** Experiments were conducted at the Institut du Développement et des Ressources en Informatique Scientifique (IDRIS) Paris, France. We thank the Nucleus for European Modeling of the Ocean (NEMO) Team for its technical support. The analysis was supported by the project CYCLOCEAN from Les Enveloppes Fluides et l'Environnement (LEFE) AO2010-538863. We thank Daniel Nethery for useful comments. We thank Kerry Emanuel and an anonymous reviewer for their useful comments that led to improve the present manuscript.

References

Ali, M. M., P. S. V. Jagadeesh, and S. Jain (2007), Effect of eddies on the Bay of Bengal cyclone intensity, *Eos Trans. AGU*, *88*, 93, doi:10.1029/2007EO080001.

Bister, M., and K. A. Emanuel (1998), Dissipative heating and hurricane intensity, *Meteorol. Atmos. Phys.*, *65*, 233–240, doi:10.1007/BF01030791.

Bosart, L. F., W. E. Bracken, J. D. Molinari, C. S. Velden, and P. G. Black (2000), Environmental influences on the rapid intensification of Hurricane Opal (1995) over the Gulf of Mexico, *Mon. Weather Rev.*, *128*, 322–352, doi:10.1175/1520-0493(2000)128<0322:EIOTRI>2.0.CO;2.

Buarque, S. R., C. Vanroyen, and C. Agier (2009), Tropical cyclone heat potential index revisited, *Mercator Ocean Q. Newsl.*, *33*, 24–30.

Chen, S., W. Zhao, and M. A. Donelan (2007), The CBLAST-Hurricane program and the next-generation fully coupled atmosphere-wave-ocean models for hurricane research and prediction, *Bull. Am. Meteorol. Soc.*, *88*, 311–317, doi:10.1175/BAMS-88-3-311.

Cione, J. J., and E. W. Uhlhorn (2003), Sea surface temperature variability in hurricanes: Implications with respect to intensity change, *Mon. Weather Rev.*, *131*, 1783–1796, doi:10.1175//2562.1.

DeMaria, M., M. Mainelli, L. K. Shay, J. A. Knaff, and J. Kaplan (2005), Further improvements to the Statistical Hurricane Intensity Prediction Scheme (SHIPS), *Weather Forecasting*, *20*, 531–543, doi:10.1175/WAF862.1.

Drevillon, M., et al. (2008), The GODAE/Mercator-Ocean global ocean forecasting system: Results, applications and prospects, *J. Oper. Oceanogr.*, *1*, 51–57.

Emanuel, K. A. (1999), Thermodynamic control of hurricane intensity, *Nature*, *401*, 665–669, doi:10.1038/44326.

Emanuel, K. A. (2003), Tropical cyclones, *Annu. Rev. Earth Planet. Sci.*, *31*, 75–104, doi:10.1146/annurev.earth.31.100901.141259.

Emanuel, K. A. (2005), Increasing destructiveness of tropical cyclones over the past 30 years, *Nature*, *436*, 686–688, doi:10.1038/nature03906.

Emanuel, K. A., C. DesAutels, C. Holloway, and R. Korty (2004), Environmental control of tropical cyclone intensity, *J. Atmos. Sci.*, *61*, 843–858, doi:10.1175/1520-0469(2004)061<0843:ECOTCI>2.0.CO;2.

Goni, G., et al. (2009), Applications of satellite-derived ocean measurements to tropical cyclone intensity forecasting, *Oceanography*, *22*, 190–197, doi:10.5670/oceanog.2009.78.

Greatbatch, R. J. (1984), On the response of the ocean to a moving storm: Parameters and scales, *J. Phys. Oceanogr.*, *14*, 59–78, doi:10.1175/1520-0485(1984)014<0059:OTROTO>2.0.CO;2.

Griffies, S., et al. (2009), Coordinated Ocean-ice Reference Experiments (COREs), *Ocean Modell.*, *26*, 1–46, doi:10.1016/j.ocemod.2008.08.007.

Hong, X., S. W. Chang, S. Raman, L. K. Shay, and R. Hodur (2000), The interaction between Hurricane Opal (1995) and a warm core ring in the Gulf of Mexico, *Mon. Weather Rev.*, *128*, 1347–1365, doi:10.1175/1520-0493(2000)128<1347:TIBHOA>2.0.CO;2.

Jacob, S. D., and L. K. Shay (2003), The role of oceanic mesoscale features on the tropical cyclone-induced mixed layer response: A case study, *J. Phys. Oceanogr.*, *33*, 649–676, doi:10.1175/1520-0485(2003)33<649:TROOMF>2.0.CO;2.

Jacob, S. D., L. K. Shay, A. J. Mariano, and P. G. Black (2000), The 3D oceanic mixed layer response to Hurricane Gilbert, *J. Phys. Oceanogr.*, *30*, 1407–1429, doi:10.1175/1520-0485(2000)030<1407:TOMLRT>2.0.CO;2.

Knapp, K. R., M. C. Kruk, D. H. Levinson, H. J. Diamond, and C. J. Neumann (2010), The International Best Track Archive for Climate Stewardship (IBTrACS): Unifying tropical cyclone data, *Bull. Am. Meteor. Soc.*, *91*, 363–376.

Knutson, T. R., J. J. Sirutis, S. T. Garner, G. A. Vecchi, and I. M. Held (2008), Simulated reduction in Atlantic hurricane frequency under twenty-first-century warming conditions, *Nat. Geosci.*, *1*, 359–364, doi:10.1038/ngeo202.

Korty, R. L., K. A. Emanuel, and J. R. Scott (2008), Tropical cyclone-induced upper-ocean mixing and climate: Application to equable climates, *J. Clim.*, *21*, 638–654.

Large, W., and S. Yeager (2009), The global climatology of an interannually varying air-sea flux data set, *Clim. Dyn.*, *33*, 341–364, doi:10.1007/s00382-008-0441-3.

Leipper, D. F., and D. Volgenau (1972), Hurricane heat potential of the Gulf of Mexico, *J. Phys. Oceanogr.*, *2*, 218–224, doi:10.1175/1520-0485(1972)002<0218:HHPOTG>2.0.CO;2.

Lengaigne, M., U. Haussman, G. Madec, C. Menkes, J. Vialard, and J. M. Molines (2012), Mechanisms controlling warm water volume interannual variations in the equatorial Pacific: Diabatic versus adiabatic processes, *Clim. Dyn.*, *38*, 1031–1046.

Liu, L. L., W. Wang, and R. X. Huang (2008), The mechanical energy input to the ocean induced by tropical cyclones, *J. Phys. Oceanogr.*, *38*, 1253–1266, doi:10.1175/2007JPO3786.1.

Lloyd, I. D., and G. A. Vecchi (2011), Observational evidence of oceanic controls on hurricane intensity, *J. Clim.*, *24*, 1138–1153, doi:10.1175/2010JCLI3763.1.

Lloyd, I. D., T. Marchok, and G. A. Vecchi (2011), Diagnostics comparing sea surface temperature feedbacks from operational hurricane forecasts to observations, *J. Adv. Model. Earth Syst.*, *3*, M11002, doi:10.1029/2011MS000075.

Locarnini, R. A., A. V. Mishonov, J. I. Antonov, T. P. Boyer, and H. E. Garcia (2006), *World Ocean Atlas 2005*, vol. 1, *Temperature*, *NOAA Atlas NESDIS*, vol. 61, edited by S. Levitus, 182 pp., NOAA, Silver Spring, Md.

Madec, G. (2008), NEMO ocean engine, *Note Pôle Modél. 27*, Inst. Pierre-Simon Laplace, Paris.

Mainelli, M., M. DeMaria, L. K. Shay, and G. Goni (2008), Application of oceanic heat content estimation to operational forecasting of recent Atlantic category 5 hurricanes, *Weather Forecasting*, *23*, 3–16, doi:10.1175/2007WAF2006111.1.

Penduff, T., M. Juza, L. Brodeau, G. C. Smith, B. Barnier, J.-M. Molines, A.-M. Treguier, and G. Madec (2010), Impact of global ocean model resolution on sea-level variability with emphasis on interannual time scales, *Ocean Sci.*, *6*, 269–284, doi:10.5194/os-6-269-2010.

Price, J. F. (1979), On the scaling of stress-driven entrainment experiments, *J. Fluid Mech.*, *90*(3), 509–529, doi:10.1017/S0022112079002366.

Price, J. F. (1981), Upper ocean response to a hurricane, *J. Phys. Oceanogr.*, *11*, 153–175, doi:10.1175/1520-0485(1981)011<0153:UORTAH>2.0.CO;2.

Price, J. F. (2009), Metrics of hurricane-ocean interaction: Vertically integrated or vertically averaged ocean temperature?, *Ocean Sci.*, *5*, 351–368, doi:10.5194/os-5-351-2009.

Riehl, H. (1950), A model of hurricane formation, *J. Appl. Phys.*, *21*, 917–925, doi:10.1063/1.1699784.

Roemmich, D., G. C. Johnson, S. Riser, R. Davis, J. Gilson, W. B. Owens, S. L. Garzoli, C. Schmid, and M. Ignaszewski (2009), The Argo program: Observing the global ocean with profiling floats, *Oceanography*, *22*, 34–43, doi:10.5670/oceanog.2009.36.

Royer, J. F., F. Chauvin, B. Timbal, P. Araspin, and D. Grimal (1998), A GCM study of the impact of greenhouse gas increase on the frequency of occurrence of tropical cyclones, *Clim. Change*, *38*, 307–343, doi:10.1023/A:1005386312622.

Schade, L. R. (2000), Tropical cyclone intensity and sea surface temperature, *J. Atmos. Sci.*, *57*, 3122–3130, doi:10.1175/1520-0469(2000)057<3122:TCIASS>2.0.CO;2.

Schade, L. R., and K. A. Emanuel (1999), The ocean's effect on the intensity of tropical cyclones: Results from a simple coupled atmosphere-ocean model, *J. Atmos. Sci.*, *56*, 642–651, doi:10.1175/1520-0469(1999)056<0642:TOSEOT>2.0.CO;2.

Sengupta, D., B. R. Goddalehundi, and D. S. Anitha (2008), Cyclone-induced mixing does not cool SST in the post-monsoon north Bay of Bengal, *Atmos. Sci. Lett.*, *9*, 1–6, doi:10.1002/asl.162.

Shay, L. K., and J. K. Brewster (2010), Oceanic heat content variability in the eastern Pacific Ocean for hurricane intensity forecasting, *Mon. Weather Rev.*, *138*, 2110–2131, doi:10.1175/2010MWR3189.1.

Shay, L. K., G. J. Goni, and P. G. Black (2000), Effects of a warm oceanic feature on Hurricane Opal, *Mon. Weather Rev.*, *128*, 1366–1383, doi:10.1175/1520-0493(2000)128<1366:EOAWOF>2.0.CO;2.

Vincent, E. M., M. Lengaigne, G. Madec, J. Vialard, G. Samson, N. C. Jourdain, C. E. Menkes, and S. Jullien (2012), Processes setting the characteristics of sea surface cooling induced by tropical cyclones, *J. Geophys. Res.*, *117*, C02020, doi:10.1029/2011JC007396.

Wentz, F. J., C. Gentemann, D. Smith, and D. Chelton (2000), Satellite measurements of sea surface temperature through clouds, *Science*, *288*, 847–850, doi:10.1126/science.288.5467.847.

Willoughby, H. E., R. W. R. Darling, and M. E. Rahn (2006), Parametric representation of the primary hurricane vortex. Part II: A new family of sectionally continuous profiles, *Mon. Weather Rev.*, *134*, 1102–1120, doi:10.1175/MWR3106.1.

Xie, S. P., H. Annamalai, F. A. Schott, and J. P. McCreary (2002), Structure and mechanisms of South Indian Ocean climate variability, *J. Clim.*, *15*(8), 864–878, doi:10.1175/1520-0442(2002)015<0864:SAMOSI>2.0.CO;2.

Yablonsky, R. M., and I. Ginis (2009), Limitation of one-dimensional ocean models for coupled hurricane-ocean model forecasts, *Mon. Weather Rev.*, *137*, 4410–4419, doi:10.1175/2009MWR2863.1.